

STEAM: Squeeze and Transform Enhanced Attention Module

Rishabh Sabharwal¹, Ram Samarth B B¹, Parikshit Singh Rathore¹, Punit Rathore¹

¹Indian Institute of Science, Bangalore, Karnataka, India
{srishabh, ramsamarthbb, parikshits, prathore}@iisc.ac.in

Abstract

Channel and spatial attention mechanisms introduced by earlier works enhance the representation abilities of deep convolutional neural networks (CNNs) but often lead to increased parameter and computation costs. While recent approaches focus solely on efficient feature context modeling for channel attention, we aim to model both channel and spatial attention comprehensively with minimal parameters and reduced computation. Leveraging the principles of relational modeling in graphs, we introduce a constant-parameter module, *STEAM: Squeeze and Transform Enhanced Attention Module*, which integrates channel and spatial attention to enhance the representation power of CNNs. To our knowledge, we are the first to propose a graph-based approach for modeling both channel and spatial attention, utilizing concepts from multi-head graph transformers. Additionally, we introduce *Output Guided Pooling* (OGP), which efficiently captures spatial context to further enhance spatial attention. We extensively evaluate STEAM for large-scale image classification, object detection and instance segmentation on standard benchmark datasets. STEAM achieves a 2% increase in accuracy over the standard ResNet-50 model with only a meager increase in GFLOPs. Furthermore, STEAM outperforms leading modules ECA and GCT in terms of accuracy while achieving a three-fold reduction in GFLOPs. The code will be made available upon acceptance.

Introduction

Convolutional Neural Networks (CNNs) have greatly advanced vision tasks due to their strong representation capabilities. However, since convolutions operate within local spatial neighborhoods, repeated local operations are required to capture large receptive fields, leading to computational and optimization challenges (Wang et al. 2018). This limitation has driven the exploration of channel and spatial attention mechanisms to capture these dependencies better. Spatial Transformer Networks (Jaderberg et al. 2015) use an adaptive mechanism to enhance spatial dependencies and NLNets (Wang et al. 2018) utilize non-local operators to capture long-range dependencies. SENet (Hu, Shen, and Sun 2018) uses adaptive recalibration of feature maps using bottleneck *multi-layer perceptrons* (MLPs) to capture channel attention. BAM (Park et al. 2018) and CBAM (Woo et al. 2018) focus on integrating channel and spatial attention to improve dependency capture.

Modules	DR	CA	SA	Parameters
SE	✓	✓	✗	$\frac{2}{r} \sum_{s=1}^S N_s \cdot C_s^2$
GCT	✗	✓	✗	$\sum_{s=1}^S N_s$
ECA	✗	✓	✗	$\sum_{s=1}^S N_s \cdot \lfloor (\log_2 C + 1) / 2 \rfloor_{odd}$
CBAM	✓	✓	✓	$\sum_{s=1}^S N_s \cdot (C_s^2 * \frac{2}{r} + k^2)$
MCA	✗	✓	✗	$\sum_{s=1}^S N_s \cdot C_s * 2$
STEAM	✗	✓	✓	Independent of C!

Table 1: Comparison with SOTA modules based on channel dimensionality reduction (DR), Channel Attention (CA) and Spatial Attention (SA), total number of parameters.

C – the number of channels; r – the reduction ratio of SE and CBAM; N_s – the number of repeated blocks in stage s ; S – the total number of stages; and k – the size of 2-D kernel used in CBAM. $\lfloor \cdot \rfloor$ indicates the nearest odd number.

The SE block in SENet captures inter-channel interactions for efficient attention but significantly increases the number of parameters. Moreover, the dimensionality reduction in fully connected layers fails to capture direct dependencies, as highlighted by ECA (Wang et al. 2020). This issue also affects methods such as CBAM (Woo et al. 2018) and GE (Hu et al. 2018), which employ SE-like dimensionality reduction techniques for modeling channel attention. Methods such as GCT (Ruan et al. 2021) utilize non-parametric strategies, whereas SRM (Lee, Kim, and Nam 2019) and MCA (Jiang et al. 2024) adopt moment-based techniques to enrich feature context and boost channel attention.

Upon assessing these studies, we find that many approaches significantly increase the number of parameters to enhance performance, while others focus on reducing parameters by concentrating solely on channel attention, as shown in Table 1. In contrast, our method employs graph relational modeling to effectively capture both channel and spatial attention, striking a balance between performance and computational efficiency. From the channel perspective, each channel can be viewed as a node with the global information of its corresponding spatial map as the feature vector. From the spatial perspective, each spatial unit, encompassing positional and interaction details, can be perceived as a node with global information across all the channels as its attribute. Therefore, channel and spatial attention can be modeled as graph attention mechanisms, which we refer to as

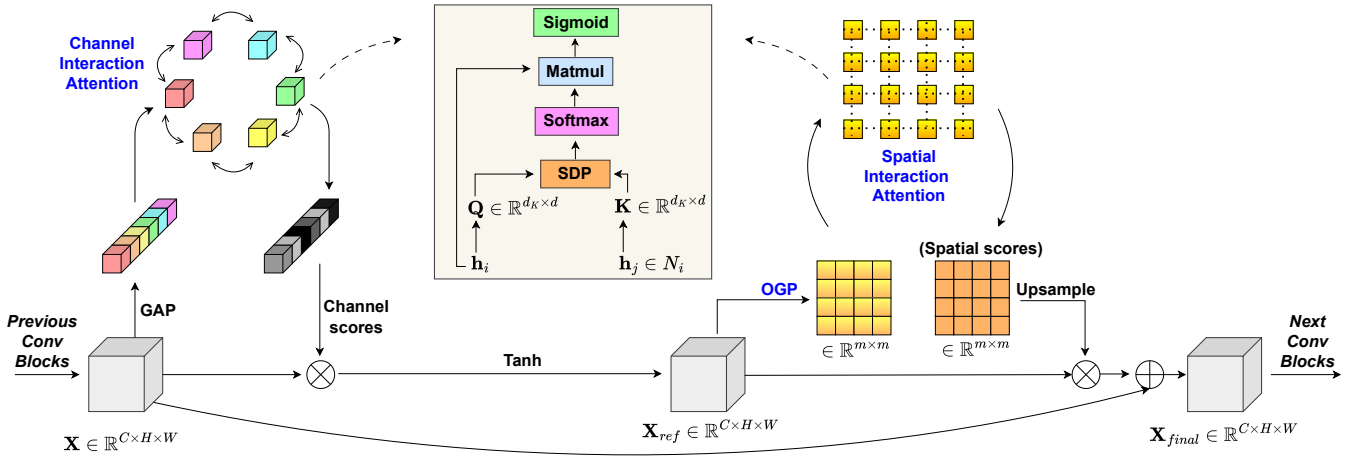


Figure 1: Detailed Overview of STEAM.

Channel Interaction Attention (CIA) and *Spatial Interaction Attention* (SIA). We introduce a new *Output Guided Pooling* (OGP) to capture spatial context efficiently which enhances our SIA. We name our approach that integrates both CIA and SIA as STEAM: *Squeeze and Transform Enhanced Attention Module*.

As evident in Table 1, STEAM leverages both channel and spatial attention without introducing dimensionality reduction in a parameter-efficient manner. Furthermore, STEAM integrates seamlessly with various network architectures, including ResNets (He et al. 2016; Xie et al. 2017) and lightweight models such as ShuffleNet (Zhang et al. 2018) and ShuffleNet-V2 (Ma et al. 2018).

In general, the key contributions of this work can be summarized as follows: (1) We develop channel and spatial attention through a graphical approach by defining channel and spatial graphs, with the goal of achieving efficient representation learning. (2) We use multi-head attention, inspired by graph transformers, to capture various relationships within channel and spatial graphs. Additionally, we introduce *Output Guided Pooling* for optimal spatial attention modeling. (3) We develop a constant-parameter module independent of the backbone it is integrated with. (4) We perform large-scale image classification on ImageNet, as well as object detection and instance segmentation on MS COCO dataset. Our experimental results demonstrate that STEAM outperforms current *state-of-the-art* (SOTA) modules, while adding minimal parameters and GFLOPs, highlighting its efficiency in terms of parameters and computation. For instance, STEAM integrated with ResNet-50 adds a minimal 320 parameters and $3.57e-3$ GFLOPs, yielding an increase of 2% Top-1 accuracy over standard ResNet-50.

Related Works

Attention Mechanism. Attention mechanisms, enhancing deeper CNNs, have been broadly explored under channel, spatial, and combined channel-spatial attention. (Zagoruyko and Komodakis 2016) introduced spatial attention function for encoding the input areas focused by the network

for decision-making. SENet (Hu, Shen, and Sun 2018) modeled channel attention by recalibrating feature maps through squeeze and excitation operations. (Roy, Navab, and Wachinger 2018) achieves consistent segmentation gains by incorporating three variants of SE modules with CNNs. GE (Hu et al. 2018) uses a gather-excite operator pair to aggregate contextual information and modulate feature maps. GCT (Ruan et al. 2021) uses a Gaussian function to excite global contexts, removing the need for parameterized contextual feature transforms. GSOP (Gao et al. 2019) employs global second-order pooling for holistic image representation, SRM (Lee, Kim, and Nam 2019) utilizes style-based pooling, and MCA (Jiang et al. 2024) combines multiple moments with Cross Moment Convolution for enhanced channel attention. Residual Attention Networks (Wang et al. 2017) enhance feature maps and increase noise resilience by computing robust 3D attention maps. CBAM (Woo et al. 2018) builds on this by independently modeling and sequentially combining channel and spatial attention mechanisms. ECA-Net (Wang et al. 2020) uses 1-D convolution to capture local cross-channel interactions, addressing dimensionality reduction issues. Approaches such as SGE (Li et al. 2019) and SANet (Zhang and Yang 2021) leverage multi-branch architecture designs similar to ShuffleNet (Zhang et al. 2018) and ShuffleNet-V2 (Ma et al. 2018) to integrate attention mechanisms. NLNet (Wang et al. 2018) employs non-local operations to capture long-range dependencies through global interactions, similar to self-attention. GCNet (Cao et al. 2019) unifies non-local and SE blocks into a *Global Context* (GC) block for enhanced context modeling. A²-Net (Chen et al. 2018) captures long-range feature interdependencies by employing universal gathering and distribution mechanisms.

Graph Neural Networks (GNNs). GNNs (Scarselli et al. 2008; He et al. 2016) model complex graph data using message passing (Gilmer et al. 2017). Advances include GCN (Kipf and Welling 2016), GAT (Veličković et al. 2017), and GraphSAGE (Hamilton, Ying, and Leskovec 2017), each employing unique aggregation techniques. The relational

inductive bias of GNNs, as explained by (Battaglia et al. 2018), makes them superior to MLPs for graph data. Attention mechanisms in GNNs have garnered significant interest: (Brody, Alon, and Yahav 2021) improved GAT with dynamic attention, (Dwivedi and Bresson 2020) introduced Graph Transformers with positional encodings, and models like SAN (Kreuzer et al. 2021), and GPS (Rampásek et al. 2022) enhanced positional and structural encoding. The application of GNNs in vision is well-reviewed in (Jiao et al. 2022). Vision GNN (Han et al. 2022), utilizes an approach similar to ViT (Dosovitskiy et al. 2020), in which each image patch is considered as a graph node that is linked to its nearest neighbors. (Aflalo et al. 2023) utilized graph spectral clustering for unsupervised image segmentation.

Proposed Method

This section provides an in-depth explanation of our Channel and Spatial Interaction Attention (CIA and SIA) mechanisms. We also describe the construction of our proposed method STEAM using these mechanisms, with a schematic diagram shown in Fig. 1.

Our initial steps towards a naïve Channel Attention

Building on ECA’s insights, we forego the dimensionality reduction strategies used in SENet, CBAM, and GE, opting for direct cross-channel attention modeling. Given the intermediate feature map $\mathbf{X} \in \mathbb{R}^{C \times H \times W}$, we treat each channel as a node, with its spatial map $\mathbf{x}_c \in \mathbb{R}^{H \times W}$ as its feature vector. We derive a correlation graph using channel-wise correlation matrix $\mathbf{A} = \mathbf{X}\mathbf{X}^T \in \mathbb{R}^{C \times C}$ computed from node features. But as CNNs deepen, the number of channels increases exponentially, resulting in large and dense graphs that pose computational challenges. Modeling such graphs requires multiple GNN layers to increase the receptive field. However, deep GNNs tend to oversmooth (Nt and Maehara 2019; Oono and Suzuki 2019), making node representations very similar, thereby degrading the performance. To avoid such dense graphs, we experimented with k -NN graphs by selecting the top k neighbors based on similarity scores, a strategy used in methods like LLE (Roweis and Saul 2000) to infer graphs. However, since we aim to model channel importance rather than similarity, k -NN graphs were found to be ineffective¹. Additionally, different correlation matrices for each image lead to excessive memory usage, hindering graph representation learning.

Exploring our Channel Interaction Mechanism

In ECA’s 1-D cross-channel convolution, the kernel size defines the local receptive field, where weighted aggregation corresponds to convolution. Drawing this analogy to graphs, the kernel size corresponds to a node’s neighborhood, with convolution modeled as message passing within this neighborhood. Inspired by these correlations, we design a channel graph G_c in which each channel is linked to its immediate 1-hop neighbors. Furthermore, the first channel is connected to the last one, creating a cyclic graph (Fig. 1).

¹refer to Table 10 in Appendix.

Therefore, $G_c = (V_c, E_c)$ denotes our channel graph with C nodes and edges, where V_c and E_c represent the vertex and edge sets respectively. $\mathbf{X}_c \in \mathbb{R}^{C \times 1}$ represents the initial node (channel) features obtained by applying *global average pooling* (GAP), a mapping $\mathbb{R}^{C \times H \times W} \mapsto \mathbb{R}^{C \times 1 \times 1}$. Given the channel graph and its associated node features, channel attention can now be effectively modeled using graph attention mechanisms. Using scaled dot-product attention (Vaswani et al. 2017) over traditional self-attention (Bahdanau, Cho, and Bengio 2014), as implemented in GAT (Veličković et al. 2017), has shown to be more effective empirically. We name this entire mechanism as *Channel Interaction Attention* (CIA) which can be computed as (Vaswani et al. 2017):

$$\mathbf{A}_{i,j}^h = \text{softmax} \left(\frac{(\mathbf{W}_K \mathbf{X}_{c_i})^T \mathbf{W}_Q \mathbf{X}_{c_j}}{d_K} \right), \forall j \in N_i \quad (1)$$

$$\mathbf{A} = \frac{1}{H} \sum_{h=1}^H \mathbf{A}^h, \mathbf{X}_{c_{att}} = \mathbf{A} \mathbf{X}_c \quad (2)$$

$$\alpha_c = \sigma(\mathbf{X}_{c_{att}}), \mathbf{X}_{ref} = \alpha_c \otimes \mathbf{X} \quad (3)$$

Here, $\mathbf{W}_K, \mathbf{W}_Q \in \mathbb{R}^{d_K \times d_{in}}$, ($d_{in} = 1$), are learnable projection matrices, where d_K specifies the dimensionality of the key and query vectors, d represents model’s hidden dimension. $\mathbf{A}_{i,j}^h$ represents the attention score between node i and its neighbor j in the h -th² head among total H heads and N_i denotes the neighborhood of node i . The final attention matrix \mathbf{A} is computed by averaging the attention scores across all H heads. The updated representation for each channel is denoted by $\mathbf{X}_{c_{att}}$ which is further processed through a sigmoid activation (σ) to produce channel scores, $\alpha_c \in \mathbb{R}^{C \times 1}$. During element-wise multiplication (denoted by \otimes in Fig. 1 and Eq. 3), α_c is broadcasted across the spatial dimension to get the modified intermediate feature map \mathbf{X}_{ref} .

Need for Spatial Attention

(Zagoruyko and Komodakis 2016) emphasizes that spatial attention is crucial for encoding key spatial regions that influence a network’s output decision. They propose a *spatial attention mapping function* (SAMF) formulated as $\mathbb{R}^{C \times H \times W} \mapsto \mathbb{R}^{H \times W}$ utilizing channel statistics. Early-layer neurons in the network activate strongly for low-level gradients, intermediate layers for distinctive features, and top layers for entire objects. Additionally, (Islam, Jia, and Bruce 2020) specifies that CNNs naturally extract positional information, with early layers capturing fine details and deeper layers focusing more on category-specific features. This inherent positional and spatial context in CNNs motivates us to use GNNs for modeling spatial attention, as they effectively capture both positional and relational information. Therefore, we construct an initial spatial graph from

²Here h represents one of the attention heads. It is not to be confused with the node representation vector denoted by \mathbf{h}_i in Fig. 1

the spatial attention map obtained by using SAMF, creating $H * W$ nodes in each stage³.

CBAM’s spatial attention module follows SAMF and incorporates 1-strided convolution to generate pixel-wise spatial scores, combining both average and max pooling across channels. However, it adds extra computations to capture finer details, thus introducing redundancy in the early stages. In order to effectively encapsulate spatial context with efficient computation, we present *Output Guided Pooling* (OGP). OGP transforms the intermediate feature map $\mathbb{R}^{C \times H \times W}$ into a fixed-size spatial map ($\in \mathbb{R}^{(m \times m)}$) using GAP along the channel dimension, where m corresponds to the dimension of the deepest spatial map (e.g., 7×7 for ResNets). This fixed-size spatial map ensures consistency across multiple layers: in deeper layers, it captures pixel-wise details, while in earlier layers, it provides adaptive spatial information at a high level. We now construct a refined spatial graph G_s using the fixed-size spatial map ($\in \mathbb{R}^{(m \times m)}$)(Fig. 2). This graph consists of m^2 nodes, where each node connects to its adjacent neighbors: central nodes have four connections, edge nodes have three, and corner nodes have two, resulting in $2m(m - 1)$ edges. $\mathbf{X}_s \in \mathbb{R}^{m^2 \times 1}$ represents the initial node feature for the spatial nodes, obtained by applying OGP on \mathbf{X}_{ref} , which is derived from our CIA module. Analogous to CIA, we leverage multi-head scaled dot-product graph attention to model spatial attention through message passing between pixels in the fixed-size spatial map. This process includes averaging attention scores across all heads, updating node representations, and applying the sigmoid σ activation to obtain initial spatial scores $\alpha_{init} \in \mathbb{R}^{m \times m}$ which are then upsampled using `torch.repeat_interleave()` (Eq. 6) to produce the final spatial scores $\alpha_s \in \mathbb{R}^{C \times H \times W}$. Modifying Eqs. 1, 2 and 3, we obtain:

$$\mathbf{A}_{i,j}^h = \text{softmax} \left(\frac{(\mathbf{W}_K \mathbf{X}_{s_i})^T \mathbf{W}_Q \mathbf{X}_{s_j}}{d_K} \right), \forall j \in N_i \quad (4)$$

$$\mathbf{A} = \frac{1}{H} \sum_{h=1}^H \mathbf{A}^h, \quad \mathbf{X}_{s_{att}} = \mathbf{A} \mathbf{X}_s \quad (5)$$

$$\alpha_{init} = \sigma(\mathbf{X}_{s_{att}}), \quad \alpha_s = \text{upsample}(\alpha_{init}) \quad (6)$$

$$\mathbf{X}_{final} = \mathbf{X} + \alpha_s \otimes \mathbf{X}_{ref} \quad (7)$$

where $\mathbf{X}_{final} \in \mathbb{R}^{C \times H \times W}$ represents the final output of STEAM, while other notations remain consistent. We note that the central submatrix ($\mathbb{R}^{(m-2) \times (m-2)}$) of our refined spatial map contains several nodes with a uniform degree of 4. This could lead to over-smoothing, as message passing among these highly interconnected nodes may result in nearly identical node representations, thereby degrading performance. To address this issue, we introduce an effective edge drop technique during model training, where one edge is randomly dropped for each node within this central submatrix. Empirical ablations in Table 5 of Appendix, demonstrate that this edge drop technique improves the model’s performance. We name this entire mechanism as *Spatial Interaction Attention* (SIA).

³For instance, ResNet-18 consists of 4 stages [c2, c3, c4, c5] with [2, 2, 2, 2] blocks in each stage.

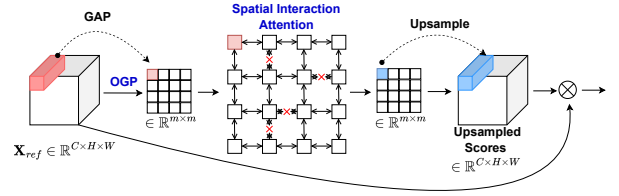


Figure 2: Spatial Interaction Attention Module.

STEAM: Squeeze and Transform Enhanced Attention Module

In this section, we introduce the final architecture. Traditional channel attention mechanisms leverage spatial representation maps, while spatial attention mechanisms draw on global channel information, highlighting the interdependence between the two. Building on this insight, we integrate our CIA and SIA modules to enhance both channel and spatial modeling simultaneously. Our empirical results from ablation studies (Table. 2) reveal that sequential arrangement outperforms the parallel one, with channel-first order yielding slightly better results than spatial-first. In our experiments, we integrate STEAM with ResNet and ShuffleNet-V2 backbones. In ResNet (stages [c2, c3, c4, c5]), we initially insert STEAM before each residual connection. For ShuffleNet-V2 (stages [c2, c3, c4]), we insert STEAM before each channel shuffle operation, as described by the authors in the Appendix of (Ma et al. 2018). Based on extensive ablations, we propose an adaptive approach (detailed in the ablations) for determining the number of STEAM units per stage, resulting in: [1, 1, 1, 1] for ResNet18; [1, 1, 2, 1] for ResNet50; [1, 1, 6, 1] for ResNet101; and [1, 2, 1] for ShuffleNet-V2. STEAM units are added at the end of each stage, and if additional units are required, they are evenly distributed within that stage⁴. This adaptive configuration, guided by experimental insights, delivers optimal results.

Parameter and Computational Complexity

In this section, we examine the parameters and computational complexity of STEAM. The parameters required for CIA and SIA are independent of the number of channels and spatial elements, as our attention modeling relies on feature vector representation, which remains consistent given a hidden model dimension d . Each of CIA and SIA contributes $4d$ parameters (since both the key and query operations contribute d for weights and biases each). As a result, a single STEAM unit introduces $8d$ parameters. The total number of parameters is given by $\sum_{s=1}^S (8d \times \lceil N_{bs}/4 \rceil)$, where S signifies the total number of stages in the model and N_{bs} indicates the number of blocks in stage s . For our experiments, we typically use $d = 8$ ⁵. As a result, incorporating all STEAM units in ResNet-50 adds $5 * (8 * 8) = 320$ parameters.

⁴Explained with diagrams in Appendix.

⁵We have experimented with multiple values of d (refer to Table 7 in Appendix).

Ablation	Type	Ad. Params	Ad. GFLOPs	Top-1	Top-5
a	ca-sa	320	3.57e-3	77.20	93.63
	sa-ca	320	3.57e-3	76.94	93.46
	ca+sa	320	3.57e-3	76.38	93.10
b	Degree-2	320	3.57e-3	77.20	93.63
	Degree-4	320	3.57e-3	76.78	93.27
c	[* , * , * , *]	1024	1.15e-2	76.87	93.38
	[0, 0, 0, *]	192	8e-4	76.71	93.28
	[1, 1, 1, 1]	256	3.13e-3	77.02	93.50
	[1, 1, 2, 1]	320	3.57e-3	77.20	93.63

Table 2: Ablations results for three standard ablations denoted by a, b and c. Ad. Params and Ad. GFLOPs indicate additional parameters and GFLOPs introduced by our module for the respective ablation experiment.

Experiments

In this section, we evaluate STEAM for large-scale image classification with ImageNet (Deng et al. 2009) and for object detection and instance segmentation with MS COCO (Lin et al. 2014). We reproduced SE, CBAM, ECA, GCT, and MCA⁶, the leading SOTA modules, for fair comparisons using the same architecture, data augmentation, and optimization parameters. All the experiments were conducted with the PyTorch framework (Paszke et al. 2019) and the MMDetection toolkit (Chen et al. 2019). In Tables 2-5, bolded values denote the best performance.

Implementation Details

In order to assess STEAM’s performance on ImageNet, we evaluate it using four well-known CNN backbones: ResNet-18, ResNet-50, ResNet-101, and ShuffleNet-V2 (with 1x scaling factor). All models were trained on 4 Nvidia RTX 4090 GPUs utilizing a mini-batch size of 256 (64 images per GPU). We apply identical training procedure across all models, including random cropping to a size of 224×224 and random horizontal flipping. We use the *Stochastic Gradient Descent* (SGD) optimizer with a momentum of 0.9 and a weight decay of $1e-4$. All models were trained for 100 epochs with an initial learning rate of 0.1, reduced by a factor of 10 at 30th, 60th, and 90th epochs. While evaluating the models on validation set, we begin by resizing the input image to 256×256 followed by a center crop of 224×224 . We report the Top-1 and Top-5 accuracy along with parameter count and GFLOPs to evaluate both storage and computational efficiency.

Furthermore, we test the efficiency of our model in object detection and instance segmentation on MS COCO dataset, employing Faster R-CNN (Ren et al. 2015), Mask R-CNN (He et al. 2017), and RetinaNet (Lin et al. 2017b) detectors, using ResNet-50 and ResNet-101 with *Feature Pyramid Network* (FPN) (Lin et al. 2017a) as backbones, initialized with weights from ImageNet classification. All models were trained using MMDetection toolkit on 4 Nvidia RTX 4090 GPUs with a mini-batch size of 8 (2 images per GPU). Pre-processing steps include resizing the shorter edge to 800

⁶The code for GCT and MCA was provided by the authors of the respective papers which helped us reproduce their results.

Methods	Params	GFLOPs	Top-1	Top-5
ResNet-18	11.69M	1.8253	69.75	89.07
+SE	+87.04K	1.8269	70.53	89.67
+CBAM	+89.86K	1.8278	70.70	89.91
+ECA	+0.04K	1.8268	70.48	89.63
+GCT	+0.01K	1.8268	71.06	89.96
+MCA	+0.78K	1.8254	70.78	89.87
+STEAM (Ours)	+0.25K	1.8261	71.36	90.10
ResNet-50	25.56M	4.1324	75.22	92.52
+SE	+2.51M	4.1460	76.61	93.18
+CBAM	+2.53M	4.1500	76.94	93.46
+ECA	+0.08K	4.1436	76.88	93.38
+GCT	+0.02K	4.1435	77.03	93.52
+MCA	+6.06K	4.1327	77.05	93.50
+STEAM (Ours)	+0.32K	4.1360	77.20	93.64
ResNet-101	44.55M	7.8651	76.71	93.26
+SE	+4.74M	7.8877	77.59	93.81
+CBAM	+4.78M	7.8942	77.90	93.87
+ECA	+0.17K	7.8832	77.85	93.88
+GCT	+0.03K	7.8830	78.08	94.15
+MCA	+130.4K	7.8656	78.17	94.18
+STEAM (Ours)	+0.57K	7.8683	78.38	94.33
ShuffleNet-V2	2.28M	0.1520	66.24	87.11
+SE	+132k	0.1547	66.92	87.65
+CBAM	+136k	0.1561	67.11	87.86
+ECA	+0.04K	0.1542	66.87	87.63
+GCT	+0.01K	0.1542	67.21	87.90
+MCA	+16.9K	0.1524	66.92	87.60
+STEAM (Ours)	+0.25K	0.1524	67.48	88.02

Table 3: Image classification results of the state-of-the-art channel attention blocks on ImageNet dataset.

while constraining the larger edge to a size of 1333, randomly flipping, and normalizing the input image. SGD with a momentum of 0.9 and weight decay of $1e-4$ was used as the optimizer. The initial learning rate was set to 0.02, decreasing by a factor of 10 at the 8th and 11th epochs, with a total of 12 epochs for training. We report *average precision* (AP), $AP_{0.5}$, $AP_{0.75}$, AP_S , AP_M , AP_L along with the number of parameters and GFLOPs to evaluate storage and computational efficiency. **NOTE:** As mentioned in our methodology, we adhere to the same adaptive strategy when incorporating STEAM into ResNet and ShuffleNet-V2 models for all experiments, unless otherwise specified. However, we introduce SE, CBAM, ECA, GCT, and MCA modules after each residual connection in ResNet and prior to each channel shuffle operation in ShuffleNet-V2.

Ablation Studies

We conduct extensive ablation studies to demonstrate the effectiveness of STEAM’s design choice. These ablations employ ResNet-50 integrated with STEAM for image classification on ImageNet dataset. Table 2 shows the results of three ablation experiments: the first evaluates the arrangement of CIA and SIA modules, the second identifies the suitable neighborhood size for CIA, and the third examines the best placement and number of STEAM units within a deep CNN. These ablations are denoted by Ablation-a, Ablation-b, and Ablation-c, respectively.

Detector	Methods	Params	GFLOPs	AP	$AP_{0.5}$	$AP_{0.75}$	AP_S	AP_M	AP_L
Faster-RCNN	ResNet-50	41.53M	207.07	36.2	57.5	39.2	20.7	39.8	46.1
	+SE (CVPR'18)	+2.51M	207.19	36.9	58.4	39.9	21.7	40.6	47.2
	+CBAM (ECCV'18)	+2.53M	207.20	37.3	59.0	40.3	21.9	41.1	47.6
	+ECA (CVPR'20)	+0.08K	207.18	37.5	59.7	40.7	21.8	41.5	47.3
	+GCT (CVPR'21)	+0.02K	207.18	37.8	60.1	41.2	22.3	41.8	47.8
	+MCA (AAAI'24)	+6.06K	207.07	37.6	59.7	40.9	22.0	41.6	47.5
	+STEAM (Ours)	+0.32K	207.07	38.1	60.3	41.2	22.5	42.2	48.3
	ResNet-101	60.52M	283.14	38.2	60.0	42.3	22.2	43.0	50.2
	+SE (CVPR'18)	+4.74M	283.33	38.5	60.7	42.2	22.5	43.7	51.0
	+CBAM (ECCV'18)	+4.78M	283.35	38.7	60.8	42.5	22.6	43.9	51.3
	+ECA (CVPR'20)	+0.17K	283.32	39.3	61.0	43.1	23.1	44.2	51.4
	+GCT (CVPR'21)	+0.03K	283.32	40.0	61.8	43.6	23.7	44.5	51.6
	+MCA (AAAI'24)	+130.4K	283.14	39.4	61.4	43.4	23.3	44.1	51.6
	+STEAM (Ours)	+0.57K	283.14	40.2	62.1	43.8	24.0	44.8	52.0
Mask-RCNN	ResNet-50	44.18M	275.58	37.0	58.8	40.6	21.3	40.7	48.3
	+SE (CVPR'18)	+2.51M	275.69	37.7	59.5	41.3	22.0	41.6	48.8
	+CBAM (ECCV'18)	+2.53M	275.70	38.0	60.3	41.6	22.2	42.1	49.5
	+ECA (CVPR'20)	+0.08K	275.69	38.2	60.1	41.6	22.3	42.1	49.3
	+GCT (CVPR'21)	+0.02K	275.69	38.7	60.6	42.1	22.8	42.7	50.0
	+MCA (AAAI'24)	+6.06K	275.58	38.3	60.3	41.8	22.5	42.5	49.5
	+STEAM (Ours)	+0.32K	275.58	39.0	61.0	42.3	23.1	43.1	50.3
	ResNet-101	63.17M	351.65	39.2	58.8	43.0	22.6	44.0	51.2
	+SE (CVPR'18)	+4.74M	351.84	39.3	60.2	43.6	23.1	44.6	51.9
	+CBAM (ECCV'18)	+4.78M	351.86	39.7	60.7	43.8	23.2	44.8	52.3
	+ECA (CVPR'20)	+0.17K	351.84	40.1	61.2	44.1	23.4	45.1	53.1
	+GCT (CVPR'21)	+0.03K	351.84	40.7	61.6	44.5	23.7	45.5	53.7
	+MCA (AAAI'24)	+130.4K	351.65	40.5	61.2	44.2	23.3	45.0	53.1
	+STEAM (Ours)	+0.57K	351.65	41.0	61.5	44.7	23.8	45.7	53.5
Retina-Net	ResNet-50	37.74M	239.32	34.9	55.0	38.1	20.1	39.3	46.1
	+SE (CVPR'18)	+2.51M	239.43	35.2	55.9	38.8	21.1	40.1	47.3
	+CBAM (ECCV'18)	+2.53M	239.44	35.6	56.3	39.0	21.3	40.7	47.6
	+ECA (CVPR'20)	+0.08K	239.43	35.9	56.4	39.3	21.3	41.0	47.8
	+GCT (CVPR'21)	+0.02K	239.43	36.7	57.0	39.5	21.7	41.2	48.1
	+MCA (AAAI'24)	+6.06K	239.32	36.1	56.8	39.5	21.5	41.1	47.9
	+STEAM (Ours)	+0.32K	239.32	37.1	57.4	39.6	21.9	41.5	48.3
	ResNet-101	56.74M	315.39	37.4	57.6	40.0	20.9	41.8	49.4
	+SE (CVPR'18)	+4.74M	315.58	37.7	57.8	41.0	21.4	42.3	50.5
	+CBAM (ECCV'18)	+4.78M	315.59	37.9	57.9	41.2	21.5	42.5	50.8
	+ECA (CVPR'20)	+0.17K	315.57	38.2	58.5	41.2	21.3	42.4	50.4
	+GCT (CVPR'21)	+0.03K	315.57	38.6	59.0	41.5	21.7	43.0	50.8
	+MCA (AAAI'24)	+130.4K	315.39	38.2	58.6	40.8	21.4	42.6	50.7
	+STEAM (Ours)	+0.57K	315.39	39.0	59.5	41.8	22.1	43.0	51.1

Table 4: Comparisons between different methods on the COCO val2017 set with object detection task.

Arrangement of CIA and SIA modules Here we perform three experiments to identify the optimum ordering of CIA and SIA modules. We employ a parallel arrangement of CIA and SIA modules (denoted as “ca+sa”) along with two sequential arrangements, CIA-first and SIA-first (denoted by “ca-sa” and “sa-ca” respectively) to evaluate the impact of different module arrangements. From Table 2, we can infer that the sequential arrangement outperforms the parallel one and a CIA-first order within the sequential arrangement slightly surpasses the SIA-first order.

Choosing the Neighborhood Size for CIA We experiment with two different node neighborhood sizes for our channel graph G_c . First, we connect each channel’s node to its direct 1-hop neighbors, giving each node 2 neighbors. We extend the neighborhood size to four by linking each node to its two preceding and two succeeding nodes (similar to ECA when

its kernel size equals 5). Observe that in both scenarios, a cyclic graph structure is formed, with each node having a degree of either two or four. As shown in Table 2, configuring each channel node with a degree of two yields better results compared to a degree of four.

Arrangement of STEAM in a deep CNN Inspired by current SOTA architectures, we initially integrated STEAM after every block within each stage of ResNet-50, which contains [3, 4, 6, 3] blocks in stages [c2, c3, c4, c5], respectively, resulting in a total of 16 STEAM units. However, empirical findings indicate that this approach produced sub-optimal performance. Following the approach described in (Srinivas et al. 2021), we added STEAM only in the final stage of ResNet-50, reducing it to 3 STEAM units. Furthermore, we tested the addition of a single STEAM unit after each stage. As shown in Table 2, adding STEAM after ev-

Methods	AP	$AP_{0.5}$	$AP_{0.75}$	AP_S	AP_M	AP_L
ResNet50	34.0	55.3	36.2	16.8	36.4	47.4
+SE	34.6	56.4	37.0	17.4	37.5	48.1
+CBAM	34.7	56.8	37.3	17.5	37.9	48.4
+ECA	35.0	57.1	37.5	18.0	38.3	48.9
+GCT	35.2	57.2	37.7	18.2	38.5	48.7
+MCA	34.8	56.9	37.5	17.7	38.1	48.5
+STEAM (Ours)	35.6	57.6	38.0	18.5	38.7	49.1
ResNet101	36.1	57.1	38.6	17.2	39.5	49.5
+SE	36.5	57.9	39.2	17.8	40.3	50.1
+CBAM	36.8	58.1	39.6	18.0	40.6	50.6
+ECA	37.2	58.5	39.5	18.3	41.2	51.0
+GCT	37.5	59.0	39.8	18.4	41.0	51.3
+MCA	37.1	58.5	39.4	18.0	40.8	50.5
+STEAM (Ours)	37.4	59.4	39.8	18.6	41.4	51.5

Table 5: Instance Segmentation using the state-of-the-art channel attention blocks on COCO val2017 set.

ery stage yielded better results compared to adding STEAM only in the final stage. Consequently, we adopted a dynamic strategy to tailor the optimal number of STEAM units per stage based on the number of blocks within that stage. Formally, the number of STEAM units per stage is given by $\lceil (N_{bs}/4) \rceil$, where N_{bs} denotes the number of blocks in a stage. Specifically, for ResNet-50, the number of STEAM units per stage is [1, 1, 2, 1].

Image Classification on ImageNet-1K

This section presents a comparison of our model against SOTA counterparts. We selected four popular backbone models, specifically ResNet-18, ResNet-50, ResNet-101 and ShuffleNet-V2. The empirical results are displayed in Table 3.

ResNet We initially assess the performance of STEAM using ResNet-18, ResNet-50, and ResNet-101 as backbone models. Table 3 clearly shows that STEAM surpasses all its counterparts across various ResNet models. Notably, in ResNet-18, STEAM achieves a 0.30% increase in Top-1 accuracy over GCT, which already outperforms other modules. For ResNet-50 and ResNet-101, STEAM surpasses the former top module, MCA, by 0.15% and 0.21% in Top-1 accuracy, respectively. Overall, STEAM provides an accuracy boost of 1.61%, 1.98%, and 1.67% over the standard ResNet-18, ResNet-50, and ResNet-101 models, respectively.

ShuffleNet-V2 We evaluated STEAM on a lightweight CNN architecture⁷, ShuffleNet-V2 as the backbone. As illustrated in Table 3, STEAM surpasses all other modules, obtaining 0.27% Top-1 accuracy gain, compared to the second-best module, GCT. In general, STEAM outperforms all the prior SOTA modules while maintaining comparable parameter and computational complexity.

Object Detection on MS COCO

We conduct object detection experiments on the MS-COCO dataset using Faster-RCNN, Mask-RCNN, and RetinaNet

detectors with ResNet-50 and ResNet-101 as backbones. We compare our approach with SE, CBAM, ECA, GCT, and MCA modules. As shown in Table 4, STEAM consistently outperforms these SOTA methods in object detection.

For Faster-RCNN with ResNet-50, STEAM improves AP by 1.9% over the baseline, with gains of 1.2% over SE, 0.8% over CBAM, 0.6% over ECA, 0.3% over GCT, and 0.5% over MCA. With ResNet-101, STEAM achieves a 2.0% increase over the baseline in AP, outperforming SE by 1.7%, CBAM by 1.5%, ECA by 0.9%, GCT by 0.2%, and MCA by 0.8%. In Mask-RCNN experiments with ResNet-50 as backbone, STEAM outperforms the baseline, SE, CBAM, ECA, GCT, and MCA, with AP gains of 2.0%, 1.3%, 1.0%, 0.8%, 0.3%, and 0.7% respectively. With ResNet-101, STEAM also surpasses these methods, achieving AP improvements of 1.8%, 1.7%, 1.3%, 0.9%, 0.3%, and 0.5%. In RetinaNet experiments with ResNet-50, STEAM outperforms the baseline, SE, CBAM, ECA, GCT, and MCA, with AP gains of 2.2%, 1.9%, 1.5%, 1.2%, 0.4%, and 1.0%. With ResNet-101, STEAM also surpasses these methods, achieving AP improvements of 1.6%, 1.3%, 1.1%, 0.8%, 0.4%, and 0.8%.

Instance Segmentation on MS-COCO dataset

Finally, we perform instance segmentation experiments on the MS-COCO dataset using Mask-RCNN as the detector and ResNet-50 and ResNet-101 as backbone models. As presented in Table 5, our proposed method, STEAM, significantly exceeds the current state-of-the-art modules. Specifically, with ResNet-50 as the backbone, STEAM surpasses the baseline, SE, CBAM, ECA, GCT, and MCA methods by improvements of 1.6%, 1.0%, 0.9%, 0.6%, 0.4%, and 0.8% AP respectively. Likewise, employing ResNet-101 as the backbone model, STEAM demonstrates superior AP performance over the baseline model, SE, CBAM, ECA, and MCA methods with increases of 1.3%, 0.9%, 0.6%, 0.2%, and 0.3% respectively. Notably, in this experiment, GCT surpasses STEAM by a marginally higher 0.1% AP score. Overall, these results highlight the effectiveness and generalization capabilities of our proposed STEAM method.

Conclusion

In this paper, we focus on learning effective channel and spatial attention for deep CNNs using a graphical approach by constructing channel and spatial graphs G_c and G_s , supported by various motivations and references. We propose CIA and SIA modules which employ multi-head scaled dot-product graph attention to capture diverse inter-channel and inter-spatial relationships respectively and introduce OGP to model spatial attention optimally. Extensive ablations support the construction of our proposed method STEAM, which efficiently models both channel and spatial attention with low parameter and computational costs. Moreover, STEAM can be seamlessly integrated with various backbones such as ResNets and lightweight models like ShuffleNet-V2. Experimental results demonstrate that STEAM outperforms previous SOTA methods in classification, object detection and instance segmentation tasks. In future research, we intend to investigate several promising di-

⁷tested with more lightweight architectures in our Appendix.

rections: (1) Integrating positional encoding into spatial attention to better capture spatial context; (2) Enhancing correlation graph learning through edge modeling techniques.

References

- Aflalo, A.; Bagon, S.; Kashti, T.; and Eldar, Y. 2023. Deepcut: Unsupervised segmentation using graph neural networks clustering. In *Proceedings of the IEEE/CVF International Conference on Computer Vision*, 32–41.
- Bahdanau, D.; Cho, K.; and Bengio, Y. 2014. Neural machine translation by jointly learning to align and translate. *arXiv preprint arXiv:1409.0473*.
- Battaglia, P. W.; Hamrick, J. B.; Bapst, V.; Sanchez-Gonzalez, A.; Zambaldi, V.; Malinowski, M.; Tacchetti, A.; Raposo, D.; Santoro, A.; Faulkner, R.; et al. 2018. Relational inductive biases, deep learning, and graph networks. *arXiv preprint arXiv:1806.01261*.
- Brody, S.; Alon, U.; and Yahav, E. 2021. How attentive are graph attention networks? *arXiv preprint arXiv:2105.14491*.
- Cao, Y.; Xu, J.; Lin, S.; Wei, F.; and Hu, H. 2019. Gnet: Non-local networks meet squeeze-excitation networks and beyond. In *Proceedings of the IEEE/CVF international conference on computer vision workshops*, 0–0.
- Chen, K.; Wang, J.; Pang, J.; Cao, Y.; Xiong, Y.; Li, X.; Sun, S.; Feng, W.; Liu, Z.; Xu, J.; et al. 2019. MMDetection: Open mmlab detection toolbox and benchmark. *arXiv preprint arXiv:1906.07155*.
- Chen, Y.; Kalantidis, Y.; Li, J.; Yan, S.; and Feng, J. 2018. A²-nets: Double attention networks. *Advances in neural information processing systems*, 31.
- Deng, J.; Dong, W.; Socher, R.; Li, L.-J.; Li, K.; and Fei-Fei, L. 2009. Imagenet: A large-scale hierarchical image database. In *2009 IEEE conference on computer vision and pattern recognition*, 248–255. Ieee.
- Dosovitskiy, A.; Beyer, L.; Kolesnikov, A.; Weissenborn, D.; Zhai, X.; Unterthiner, T.; Dehghani, M.; Minderer, M.; Heigold, G.; Gelly, S.; et al. 2020. An image is worth 16x16 words: Transformers for image recognition at scale. *arXiv preprint arXiv:2010.11929*.
- Dwivedi, V. P.; and Bresson, X. 2020. A generalization of transformer networks to graphs. *arXiv preprint arXiv:2012.09699*.
- Gao, Z.; Xie, J.; Wang, Q.; and Li, P. 2019. Global second-order pooling convolutional networks. In *Proceedings of the IEEE/CVF Conference on computer vision and pattern recognition*, 3024–3033.
- Gilmer, J.; Schoenholz, S. S.; Riley, P. F.; Vinyals, O.; and Dahl, G. E. 2017. Neural message passing for quantum chemistry. In *International conference on machine learning*, 1263–1272. PMLR.
- Hamilton, W.; Ying, Z.; and Leskovec, J. 2017. Inductive representation learning on large graphs. *Advances in neural information processing systems*, 30.
- Han, K.; Wang, Y.; Guo, J.; Tang, Y.; and Wu, E. 2022. Vision gnn: An image is worth graph of nodes. *Advances in neural information processing systems*, 35: 8291–8303.
- He, K.; Gkioxari, G.; Dollár, P.; and Girshick, R. 2017. Mask r-cnn. In *Proceedings of the IEEE international conference on computer vision*, 2961–2969.
- He, K.; Zhang, X.; Ren, S.; and Sun, J. 2016. Deep residual learning for image recognition. In *Proceedings of the IEEE conference on computer vision and pattern recognition*, 770–778.
- Hu, J.; Shen, L.; Albanie, S.; Sun, G.; and Vedaldi, A. 2018. Gather-excite: Exploiting feature context in convolutional neural networks. *Advances in neural information processing systems*, 31.
- Hu, J.; Shen, L.; and Sun, G. 2018. Squeeze-and-excitation networks. In *Proceedings of the IEEE conference on computer vision and pattern recognition*, 7132–7141.
- Islam, M. A.; Jia, S.; and Bruce, N. D. 2020. How much position information do convolutional neural networks encode? *arXiv preprint arXiv:2001.08248*.
- Jaderberg, M.; Simonyan, K.; Zisserman, A.; et al. 2015. Spatial transformer networks. *Advances in neural information processing systems*, 28.
- Jiang, Y.; Jiang, Z.; Han, L.; Huang, Z.; and Zheng, N. 2024. MCA: Moment Channel Attention Networks. In *Proceedings of the AAAI Conference on Artificial Intelligence*, volume 38, 2579–2588.
- Jiao, L.; Chen, J.; Liu, F.; Yang, S.; You, C.; Liu, X.; Li, L.; and Hou, B. 2022. Graph representation learning meets computer vision: A survey. *IEEE Transactions on Artificial Intelligence*, 4(1): 2–22.
- Kipf, T. N.; and Welling, M. 2016. Semi-supervised classification with graph convolutional networks. *arXiv preprint arXiv:1609.02907*.
- Kreuzer, D.; Beaini, D.; Hamilton, W.; Létourneau, V.; and Tossou, P. 2021. Rethinking graph transformers with spectral attention. *Advances in Neural Information Processing Systems*, 34: 21618–21629.
- Lee, H.; Kim, H.-E.; and Nam, H. 2019. Srm: A style-based recalibration module for convolutional neural networks. In *Proceedings of the IEEE/CVF International conference on computer vision*, 1854–1862.
- Li, X.; Wang, W.; Hu, X.; and Yang, J. 2019. Selective kernel networks. In *Proceedings of the IEEE/CVF conference on computer vision and pattern recognition*, 510–519.
- Lin, T.-Y.; Dollár, P.; Girshick, R.; He, K.; Hariharan, B.; and Belongie, S. 2017a. Feature pyramid networks for object detection. In *Proceedings of the IEEE conference on computer vision and pattern recognition*, 2117–2125.
- Lin, T.-Y.; Goyal, P.; Girshick, R.; He, K.; and Dollár, P. 2017b. Focal loss for dense object detection. In *Proceedings of the IEEE international conference on computer vision*, 2980–2988.
- Lin, T.-Y.; Maire, M.; Belongie, S.; Hays, J.; Perona, P.; Ramanan, D.; Dollár, P.; and Zitnick, C. L. 2014. Microsoft coco: Common objects in context. In *Computer Vision—ECCV 2014: 13th European Conference, Zurich, Switzerland, September 6–12, 2014, Proceedings, Part V 13*, 740–755. Springer.

- Ma, N.; Zhang, X.; Zheng, H.-T.; and Sun, J. 2018. Shufflenet v2: Practical guidelines for efficient cnn architecture design. In *Proceedings of the European conference on computer vision (ECCV)*, 116–131.
- Nt, H.; and Maehara, T. 2019. Revisiting graph neural networks: All we have is low-pass filters. *arXiv preprint arXiv:1905.09550*.
- Oono, K.; and Suzuki, T. 2019. Graph neural networks exponentially lose expressive power for node classification. *arXiv preprint arXiv:1905.10947*.
- Park, J.; Woo, S.; Lee, J.-Y.; and Kweon, I. S. 2018. Bam: Bottleneck attention module. *arXiv preprint arXiv:1807.06514*.
- Paszke, A.; Gross, S.; Massa, F.; Lerer, A.; Bradbury, J.; Chanan, G.; Killeen, T.; Lin, Z.; Gimelshein, N.; Antiga, L.; et al. 2019. Pytorch: An imperative style, high-performance deep learning library. *Advances in neural information processing systems*, 32.
- Rampášek, L.; Galkin, M.; Dwivedi, V. P.; Luu, A. T.; Wolf, G.; and Beaini, D. 2022. Recipe for a general, powerful, scalable graph transformer. *Advances in Neural Information Processing Systems*, 35: 14501–14515.
- Ren, S.; He, K.; Girshick, R.; and Sun, J. 2015. Faster r-cnn: Towards real-time object detection with region proposal networks. *Advances in neural information processing systems*, 28.
- Roweis, S. T.; and Saul, L. K. 2000. Nonlinear dimensionality reduction by locally linear embedding. *science*, 290(5500): 2323–2326.
- Roy, A. G.; Navab, N.; and Wachinger, C. 2018. Recalibrating fully convolutional networks with spatial and channel “squeeze and excitation” blocks. *IEEE transactions on medical imaging*, 38(2): 540–549.
- Ruan, D.; Wang, D.; Zheng, Y.; Zheng, N.; and Zheng, M. 2021. Gaussian context transformer. In *Proceedings of the IEEE/CVF Conference on Computer Vision and Pattern Recognition*, 15129–15138.
- Scarselli, F.; Gori, M.; Tsoi, A. C.; Hagenbuchner, M.; and Monfardini, G. 2008. The graph neural network model. *IEEE transactions on neural networks*, 20(1): 61–80.
- Srinivas, A.; Lin, T.-Y.; Parmar, N.; Shlens, J.; Abbeel, P.; and Vaswani, A. 2021. Bottleneck transformers for visual recognition. In *Proceedings of the IEEE/CVF conference on computer vision and pattern recognition*, 16519–16529.
- Vaswani, A.; Shazeer, N.; Parmar, N.; Uszkoreit, J.; Jones, L.; Gomez, A. N.; Kaiser, Ł.; and Polosukhin, I. 2017. Attention is all you need. *Advances in neural information processing systems*, 30.
- Veličković, P.; Cucurull, G.; Casanova, A.; Romero, A.; Lio, P.; and Bengio, Y. 2017. Graph attention networks. *arXiv preprint arXiv:1710.10903*.
- Wang, F.; Jiang, M.; Qian, C.; Yang, S.; Li, C.; Zhang, H.; Wang, X.; and Tang, X. 2017. Residual attention network for image classification. In *Proceedings of the IEEE conference on computer vision and pattern recognition*, 3156–3164.
- Wang, Q.; Wu, B.; Zhu, P.; Li, P.; Zuo, W.; and Hu, Q. 2020. ECA-Net: Efficient channel attention for deep convolutional neural networks. In *Proceedings of the IEEE/CVF conference on computer vision and pattern recognition*, 11534–11542.
- Wang, X.; Girshick, R.; Gupta, A.; and He, K. 2018. Non-local neural networks. In *Proceedings of the IEEE conference on computer vision and pattern recognition*, 7794–7803.
- Woo, S.; Park, J.; Lee, J.-Y.; and Kweon, I. S. 2018. Cbam: Convolutional block attention module. In *Proceedings of the European conference on computer vision (ECCV)*, 3–19.
- Xie, S.; Girshick, R.; Dollár, P.; Tu, Z.; and He, K. 2017. Aggregated residual transformations for deep neural networks. In *Proceedings of the IEEE conference on computer vision and pattern recognition*, 1492–1500.
- Zagoruyko, S.; and Komodakis, N. 2016. Paying more attention to attention: Improving the performance of convolutional neural networks via attention transfer. *arXiv preprint arXiv:1612.03928*.
- Zhang, Q.-L.; and Yang, Y.-B. 2021. Sa-net: Shuffle attention for deep convolutional neural networks. In *ICASSP 2021-2021 IEEE International Conference on Acoustics, Speech and Signal Processing (ICASSP)*, 2235–2239. IEEE.
- Zhang, X.; Zhou, X.; Lin, M.; and Sun, J. 2018. Shufflenet: An extremely efficient convolutional neural network for mobile devices. In *Proceedings of the IEEE conference on computer vision and pattern recognition*, 6848–6856.

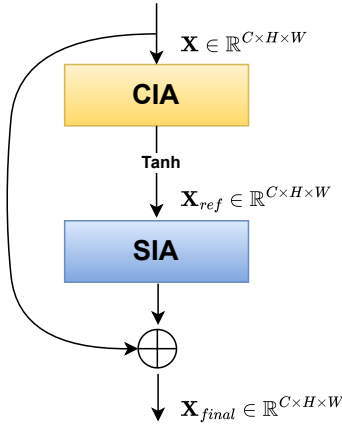


Figure 3: Overview of STEAM

Appendix

STEAM Configuration

In this section, we discuss the overall configuration of our proposed method, STEAM. Table 6 provides the configuration details for both the CIA and SIA modules. Additionally, we introduce a fixed \tanh non-linearity between the CIA and SIA modules. The value of d_K (which determines the dimension for \mathbf{W}_K and \mathbf{W}_Q referenced in Eqs. 1 and 4) is not explicitly stated, but is often defined as d/H , which equals 2 for both CIA and SIA, where H denotes the total number of heads. An overview of STEAM is shown in Fig. 3

For the placement of STEAM units in ResNets and ShuffleNet-V2, we adopt the same adaptive strategy discussed in the methodology section. To better understand our adaptive strategy, we have illustrated how STEAM is integrated in a standard ResNet-18 (Fig. 4). ResNet-18 contains [2, 2, 2, 2] blocks in stages [c2, c3, c4, c5], hence the number of STEAM units for each stage will be $\lceil 2/4 \rceil = 1$. Thus, the number of STEAM units per stage for ResNet-18 are [1, 1, 1, 1], implying that only one STEAM unit needs to be added in every stage, hence we position it at the end of each stage.

Similarly, ResNet-50 contains [3, 4, 6, 3] blocks in stages [c2, c3, c4, c5], hence the number of STEAM units for each stage will be $\lceil 3/4 \rceil$, $\lceil 4/4 \rceil$, $\lceil 6/4 \rceil$, $\lceil 3/4 \rceil$ which equals to [1, 1, 2, 1] respectively. Stages c2, c3, and c5 require only one STEAM unit. Hence we position our module at the end of these stages (Figs. 5, 6, 8). For stage c4, two STEAM units are needed. To ensure uniform placement, one unit is added at the end of the stage, and the other is placed after the 3rd block (Fig. 7). This pattern is consistently applied to both the ResNet-101 and ShuffleNet-V2 models. Fig. 9 shows AlexNet integrated with STEAM. We have omitted the batch normalization, pooling, and activation layers in Figs. 2-7 to keep the illustrations simple. Readers are encouraged to refer to (He et al. 2016) and (?) for the exact architectural details of ResNets and AlexNet, respectively.

Ablations

In this section, we conduct extensive ablations to identify the optimal mechanisms and hyperparameters for designing our proposed method, STEAM: *Squeeze and Transform Enhanced Attention Module*. For these ablations, we use ResNet-18 as a backbone integrated with STEAM and evaluate its effectiveness on image classification using a subset of the ImageNet dataset, consisting of 100 randomly selected classes, forming the ImageNet-100 subset (as shown in Table 7), with approximately 128K training images and 5K validation images. The selected 100 classes are the same as those used by (?). We report Top-1 and Top-5 accuracy for all ablations in Tables 3-11 where bolded values denote the best performance.

We study the following ablations:

- Effect of different pooling techniques used in CIA module (Table 8).
- Effect of different pooling techniques used in SIA module (Table 9).
- Effect of random edge drop in SIA (Table 10).
- Effect of different activation functions used between CIA and SIA (Table 11).
- Effect of d and H on STEAM (Table 12).
- Comparison of STEAM with it’s SOTA counterparts on ImageNet-100 (Table 13).
- Effect of Output Guided Pooling on CBAM (Table 14).
- Comparison of naïve channel attention with our proposed CIA module (Table 15).
- Comparison of STEAM with it’s SOTA counterparts on ImageNet-100 using a lightweight model, AlexNet (Table 16).

Implementation Details

We follow the same adaptive strategy for integrating STEAM in ResNet-18 whereas we add SE, CBAM, ECA, GCT and MCA modules before every residual connection in ResNet-18. All the models were trained on a single NVIDIA RTX 4090 GPU using a mini-batch size of 256. We applied identical training procedure for all the models, including random cropping to a size of 224×224 and random horizontal flipping. We use the *Stochastic Gradient Descent* (SGD) optimizer with a momentum of 0.9 and a weight decay of $1e-4$. All models were trained for 50 epochs with an initial learning rate of 0.1 which was decremented by a factor of 10 at 20^{th} , 40^{th} epochs. While evaluating the models on validation set, we begin by resizing the input image to 256×256 followed by a center crop of 224×224 and random horizontal flipping. **NOTE:** We follow the same training configuration for all the ablation experiments unless otherwise specified.

Pooling techniques in CIA First, we examine the impact of various pooling mechanisms in the CIA, specifically global average pooling, global max pooling, and a combination of both through concatenation. As shown in Table 8, global average pooling results in slightly better Top-1 accuracy compared to the concatenation of global average and

Parameter	Channel Interaction Attention (CIA)	Spatial Interaction Attention (SIA)
Pooling mechanism	GAP	OGP with output size fixed to 7×7
Node degree	Fixed to 2 for each node	2 - corner, 3 - edge and 4 - central nodes
d	8	8
H	4	4
Edge drop used	No	Yes (only for central submatrix)
Upsampling technique	NA	<code>torch.repeat_interleave()</code>

Table 6: Parameters and their values for CIA and SIA modules.

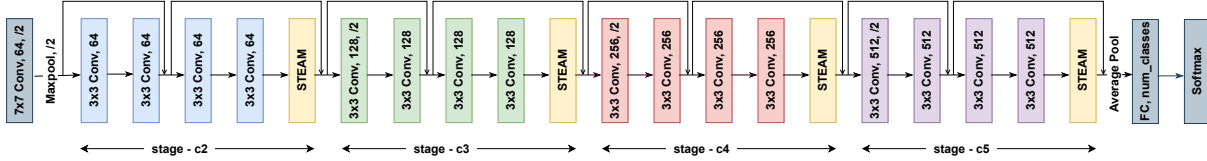


Figure 4: ResNet-18 integrated with STEAM

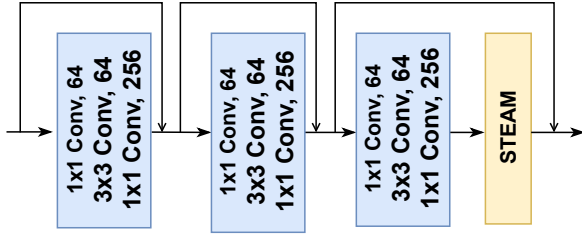


Figure 5: Stage c2 of ResNet-50 integrated with STEAM.

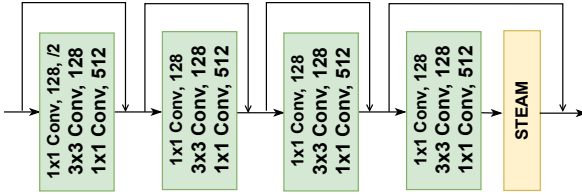


Figure 6: Stage c3 of ResNet-50 integrated with STEAM.

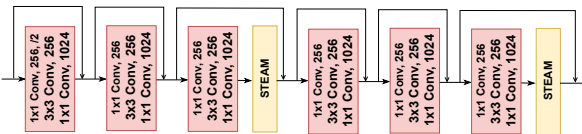


Figure 7: Stage c4 of ResNet-50 integrated with STEAM.

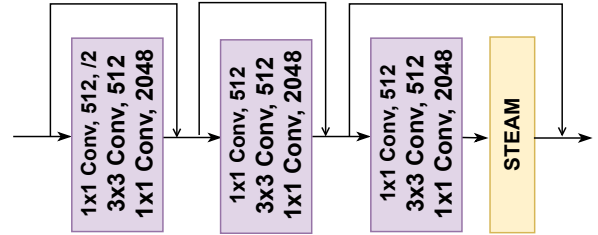


Figure 8: Stage c5 of ResNet-50 integrated with STEAM.

max pooling. However, global max pooling produced sub-optimal results.

Pooling techniques in SIA Next, we assess the effects of various pooling mechanisms in SIA, including global max pooling, global average pooling, and their combination via concatenation. Consistent with the CIA results, global average pooling yields slightly better Top-1 accuracy compared to the other approaches. The results of this ablation are presented in Table 9.

Effect of random edge drop in SIA As discussed in the methodology, we hypothesized that several nodes having a uniform degree of 4 within the central submatrix of our refined spatial map could lead to over-smoothing, resulting in identical node representations and degrading the model’s performance. To investigate this, we performed two ablations: one without random edge drop and another with random edge drop applied specifically to nodes in the central submatrix within SIA. Table 10 demonstrates that applying random edge drop to these nodes does, in fact, improve the model’s performance.

Different activation functions Next, we examine the impact of different non-linearities (activations) used between our CIA and SIA modules. We hypothesize that introducing non-linearity between these two modules can enhance the model’s ability to capture more complex relationships.

ImageNet-100 Classes									
n02869837	n01749939	n02488291	n02107142	n13037406	n02091831	n04517823	n04589890	n03062245	n01773797
n01735189	n07831146	n07753275	n03085013	n04485082	n02105505	n01983481	n02788148	n03530642	n04435653
n02086910	n02859443	n13040303	n03594734	n02085620	n02099849	n01558993	n04493381	n02109047	n04111531
n02877765	n04429376	n02009229	n01978455	n02106550	n01820546	n01692333	n07714571	n02974003	n02114855
n03785016	n03764736	n03775546	n02087046	n07836838	n04099969	n04592741	n03891251	n02701002	n03379051
n02259212	n07715103	n03947888	n04026417	n02326432	n03637318	n01980166	n02113799	n02086240	n03903868
n02483362	n04127249	n02089973	n03017168	n02093428	n02804414	n02396427	n04418357	n02172182	n01729322
n02113978	n03787032	n02089867	n02119022	n03777754	n04238763	n02231487	n03032252	n02138441	n02104029
n03837869	n03494278	n04136333	n03794056	n03492542	n02018207	n04067472	n03930630	n03584829	n02123045
n04229816	n02100583	n03642806	n04336792	n03259280	n02116738	n02108089	n03424325	n01855672	n02090622

Table 7: 100 classes randomly sampled from ImageNet to create ImageNet-100 dataset.

Pooling Mechanism	Top-1	Top-5
Global Average Pool (GAP)	81.14	94.79
Global Max Pool (GMP)	80.57	94.82
Concatenation (GAP & GMP)	80.85	94.73

Table 8: Effect of different pooling techniques used in CIA.

Pooling Mechanism	Top-1	Top-5
Global Average Pool (GAP)	81.14	94.79
Global Max Pool (GMP)	80.46	94.70
Concatenation (GAP & GMP)	80.95	94.85

Table 9: Effect of different pooling techniques used in SIA.

Empirical results, as shown in Table 11, clearly indicate that incorporating any non-linearity is better than none, leading to improved Top-1 accuracy. Among ReLU, Tanh, and Sigmoid, we find that Tanh yields the best results.

Effect of d and H on STEAM Next, we discuss the effect of d , the hidden dimension and H , the number of heads used in our multi-head graph attention. We experiment with the following pairs of (d, H) s: (4, 1), (4, 2), (8, 1), (8, 4), (8, 8), (16, 1), (16, 4), (16, 8). Table 12 shows that using $(d = 8, H = 4)$ yields slightly better Top-1 accuracy than $(d = 8, H = 8)$ but the latter achieves better Top-5 accuracy.

Comparison with SOTA modules on ImageNet-100 After identifying the optimal parameters for our module, we proceed to compare STEAM with its SOTA counterparts—SE, CBAM, ECA, GCT, and MCA. As shown in Table 13, STEAM outperforms all these leading modules on our ImageNet-100 dataset, demonstrating the effectiveness of our approach even on smaller datasets. Specifically, STEAM achieves a 1.34%, 0.82%, 0.49%, 0.66%, 0.29%, and 0.17% higher Top-1 accuracy compared to the standard ResNet-18, SE, CBAM, ECA, GCT, and MCA methods, respectively.

Effect of Output Guided Pooling Next, we analyze the effectiveness of our proposed *Output Guided Pool-*

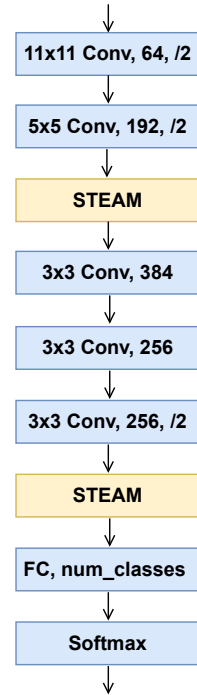


Figure 9: AlexNet integrated with STEAM

Edge Drop in SIA	Top-1	Top-5
No	80.58	94.36
Yes	81.14	94.79

Table 10: Effect of random edge drop in SIA.

Non-linearity used	Top-1	Top-5
Nothing	80.31	94.48
ReLU	80.52	94.71
Tanh	81.14	94.79
Sigmoid	80.64	94.69

Table 11: Effect of different non-linearity used between CIA and SIA.

ing (OGP). OGP transforms the intermediate feature map $\mathbb{R}^{C \times H \times W}$ into a fixed-size spatial map ($\in \mathbb{R}^{m \times m}$) using global average pooling (GAP) along the channel dimension, where m corresponds to the spatial dimension of the deepest layer. For both ResNet and ShuffleNet-V2 models, $m = 7$. Applying spatial interaction attention (SIA) directly to the intermediate feature map $\mathbb{R}^{C \times H \times W}$ would result in $H * W$ nodes, which can be computationally expensive for early layers and lead to unnecessary overhead (as discussed in the methodology). To evaluate the effectiveness of OGP, we integrate it into the spatial attention module of CBAM and train the model from scratch. Similar to STEAM, the spatial attention module of CBAM now generates spatial scores $\in \mathbb{R}^{m \times m}$, which are then upsampled using `torch.repeat_interleave()` to produce the final spatial scores $\in \mathbb{R}^{C \times H \times W}$. Table 14 shows that incorporating OGP into the spatial attention module of CBAM results in a 0.22% improvement in Top-1 accuracy compared to the standard CBAM.

Comparison with our naïve channel attention module As described in the methodology, due to the challenges associated with using dense graphs, we experimented with k -NN graphs where k was set to 16, 32, and 64. For these experiments, we used ResNet-18 as the backbone and integrated only the k -NN graph (we refer to this configuration as the k -CAM : k -Channel Attention Module) and our proposed channel attention module, excluding the SIA module. As shown in Table 15, the k -NN channel attention module (across different values of k) delivers suboptimal results compared to our proposed CIA module.

Comparison with a lightweight model Next, we evaluate the effectiveness of our module with a lightweight model, AlexNet, on the ImageNet-100 dataset. We use a standard AlexNet but replace its two fully connected layers with a single fully connected layer. As shown in Fig. 9, AlexNet is integrated with STEAM, where we add two STEAM units, after the second and fifth convolutional layer. We replace STEAM with SE, CBAM, ECA, GCT, and MCA modules when training these respective models. For the standard AlexNet, these modules are simply omitted during

d	H	Top-1	Top-5
4	1	80.45	94.61
4	2	80.57	94.64
8	1	80.75	94.69
8	4	81.14	94.79
8	8	81.02	94.88
16	1	80.61	94.70
16	4	80.98	94.90
16	8	80.77	94.67

Table 12: Effect of d and H on STEAM.

Method	Top-1	Top-5
ResNet-18	79.80	94.27
+SE	80.32	94.52
+CBAM	80.65	94.67
+ECA	80.48	94.58
+GCT	80.85	94.73
+MCA	80.97	94.68
+STEAM	81.14	94.79

Table 13: Image classification results on ImageNet-100 using ResNet-18 as backbone.

training. Table 16 shows that STEAM outperforms all its SOTA counterparts even on lightweight model like AlexNet.

Method	Top-1	Top-5
CBAM	80.65	94.67
CBAM with OGP	80.87	94.72

Table 14: Effect of OGP on CBAM.

Module	Top-1	Top-5
16-CAM ($k=16$)	80.11	94.42
32-CAM ($k=32$)	80.18	94.45
64-CAM ($k=64$)	79.96	94.31
CIA	80.56	94.80

Table 15: Comparison of naïve channel attention and our proposed CIA module.

Method	Top-1	Top-5
ResNet-18	65.74	87.02
+SE	66.19	87.61
+CBAM	66.63	88.24
+ECA	66.25	87.60
+GCT	67.02	88.14
+MCA	66.78	87.90
+STEAM	67.26	87.95

Table 16: Image classification results on ImageNet-100 using AlexNet as backbone.